
Article:
Forrester, J. orcid.org/0000-0002-8102-7576, Davidson, J., Foster, M. et al. (1 more author) (2022) Circuit simulator compatible model for the ring-dot piezoelectric transformer. Journal of Microelectromechanical Systems, 32 (1). pp. 103-116. ISSN 1057-7157

https://doi.org/10.1109/JMEMS.2022.3220042

Circuit simulator compatible model for the ring-dot piezoelectric transformer

Jack Forrester, Jonathan N. Davidson, Martin P. Foster, David A. Stone

***Abstract*—A lumped-element equivalent circuit model for the ring-dot piezoelectric transformer (PT) is derived based on a one-dimensional analysis of the radial vibration mode. Initially, equations for the magnitudes of force, vibration velocity at the boundaries of each section of the device are derived based on the piezoelectric constitutive equations and using Kirchhoff plate theory. Similarly, equations for the amplitudes of input and output currents are derived from the electric displacement field and Gauss' law. From this analytical approach, an equivalent circuit model is developed and, using a Taylor expansion, approximated as the Mason equivalent circuit. A key contribution of this work is the development of a circuit simulator compatible model which can be used by electronic engineers, without in-depth knowledge of the underlying material science, to design ring-dot PTs for power conversion applications. The resulting model is verified against both COMSOL finite element simulations and experimental impedance measurements. Compared to COMSOL, the model estimates the resonant circuit elements to within 1% and the input and output capacitance are estimated to within 10%. Experimental results match the simulation to within 10% for most parameters, and 1% for resonant frequency.**

Index Terms—Piezoelectric devices, Resonant power conversion, Modelling

I. I. Introductions

Piezoelectric transformers (PTs) are devices made with one or more sections of piezoelectric material in which vibration is used to transfer energy from the input to the output section. PTs are often compared with small, high frequency magnetic transformers PTs but they offer numerous advantages over their magnetic counterparts. These include high power density, high efficiency, and the ability to be used in adverse conditions such as high magnetic fields or high temperatures. These advantages, coupled with an integrated resonant tank circuit, mean that PTs are ideal for use in resonant converters, especially for applications such as in MRI machines, LED lighting and in the oil and aerospace industry where high-temperature operation is unavoidable [1], [2]. These advantages explain the recent academic interest in piezoelectric devices [3]–[8].

Typically, PTs have been used in low power (<5W) step-up applications (e.g. Rosen PTs); however, improvements in piezoelectric materials in the last few decades have meant that high-power (5W-50W) step-down PTs are becoming more popular. A significant barrier to the adoption of PTs in electrical converter applications is the disconnect between the models and typical parameters (e.g. tan delta) used by materials scientists who typically develop materials and construction methods, and the circuit-based models and parameters (e.g. damping resistance, Q factor) used by electronic engineers who must integrate the model with circuit-based simulation tools. This paper aims to close the gap between the disciplines by using materials science analytical techniques to derive a circuit-simulator compatible model for the ring-dot piezoelectric transformer. This approach will allow the electric engineer to design suitable power electronics circuitry to use the PT and, using appropriate inverse methods, specify the geometry and material properties of a PT for an application.

Most of the work on higher power PTs has been focused on the multi-layer radial-mode Transoner PT, which was patented in 2001 by *Face International Corp* [9]. However, many alternative topologies have been proposed [10], [11]. One topology, a unipoled disc with concentric electrodes, commonly known as the ring-dot PT was patented by Jaffe and Berlincourt in 1961[12]. The ring-dot PT has several advantages over the radial-mode Transoner PT, including ease of manufacture and reduced density of spurious modes [13].

Laoratanakul et al [14] published the first experimental results from a practical ring-dot PT. The resulting PT exhibited a power density of 18.5W/cm^3, around 10 times higher than the Rosen PT but lower than the radial-mode Transoner PT. Priya et al [15] then improved on this by building a ring-dot device with a 40W/cm^3 power density utilising an improved material and higher temperature rise. Impressively, this is the same power density as is often seen in radial-mode Transoner PTs [11]. Additionally, Priya et al proposed a multi-layer device based on a ring-dot electrode structure; however, this structure meant that heat was harder to remove from the device, thus leading to a lower power density than the single-disc variant. Guo et al [16] built and tested a lead-free ring-dot PT, showing promising results, but not quite with the same performance as PZT devices. Půlpán [13] experimentally analysed the effect of different electrode patterns on the key electrical performance characteristics. Whilst all patterns worked, with some providing improved characteristics in specific quantities, the ring-dot pattern proved to be the best overall electrode shape.

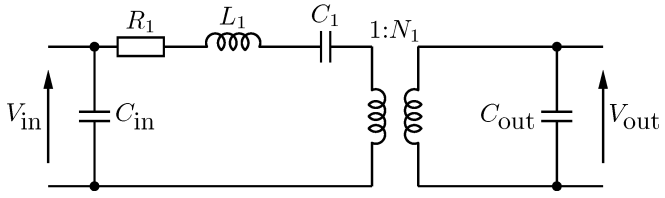

Fig. 1. Mason equivalent circuit model

The electrical behaviour of any PT can be modelled using the simplified Mason equivalent circuit model, as shown in Fig. 1. Using this equivalent circuit, a PT's electrical behaviour can be simulated using mathematical or circuit-simulation methods.

Although the electrical equivalent circuit parameters of a PTs can be measured experimentally using a variety of impedance spectroscopy methods [17], it is beneficial to be able to analytically estimate the electrical parameters of a PT from its physical design. This allows a PT to be designed for a specific electrical application and to meet specific operational requirements such as achieving zero-voltage switching for all loads in inductorless operation of half-bridge inverters, the criterion for which was reported in [18].

Equivalent circuit modelling has been performed for a variety of PT topologies [19], [20]. Půlpán *et al* [21], [22] developed a model of the voltage gain and electrical efficiency of the ring-dot PT. Ho [23] modelled the ring-dot PT using Hamilton's principle, allowing him to generate equations for the electrical performance of the PT, including input power, electrical efficiency, gain and equations for each of the equivalent circuit parameters. However, in [21]–[23] the impact of the 'gap' section between dot and ring electrodes is not explicitly considered.

This paper will present a full derivation of the lumped element circuit model of a galvanically isolated ring-dot PT, including the effect of the 'gap' section. This analysis uses an alternative method to that presented in [23], where we derive full equations for the impedance of the PT and its individual elements, by analysing the forces acting upon the PT during vibration, compared to approximating the equivalent circuit properties using Hamilton's principal as in [23]. Based on the PTs impedance, a lumped-equivalent circuit analysis is performed to generate equations for the Mason equivalent circuit properties. The testing presented here proves the effectiveness of this type of method for analysing this PT topology, contrasting the opinion in [23] where it was theorised this method would be inaccurate for the ring-dot PT.

Several improvements upon the modelling performed in [23] are presented. Firstly, in the analysis presented here, each section (input, output and gap) of the ring-dot PT is analysed individually (including the gap region), compared to an analysis of the PT as a whole as in [23]. Thus, some of the non-linear behaviour associated with each section is retained until later in the analysis thereby allowing the interactions between the different sections to be more accurately modelled. Limitations associated with the Mason equivalent circuit mean that effects of the many nonlinearities are lost in the model presented in [23]. Finally, the model in [23] requires significant mathematical analysis and piezoelectric specific knowledge from the reader to be able to generate Mason equivalent circuit component values from the dimensions of a PT and material properties. In contrast, fully solved equations for the lumped equivalent circuit properties are presented here, allowing the reader to simply input details about the PT (dimensions and material properties) and estimate the lumped equivalent circuit properties, with minimal mathematic effort. This is important for resonant converter designers, as it requires minimal knowledge of piezoelectric devices, to be able to generate equivalent circuit properties from a physical PT design, thus easing the design process for this PT topology.

II. Scope

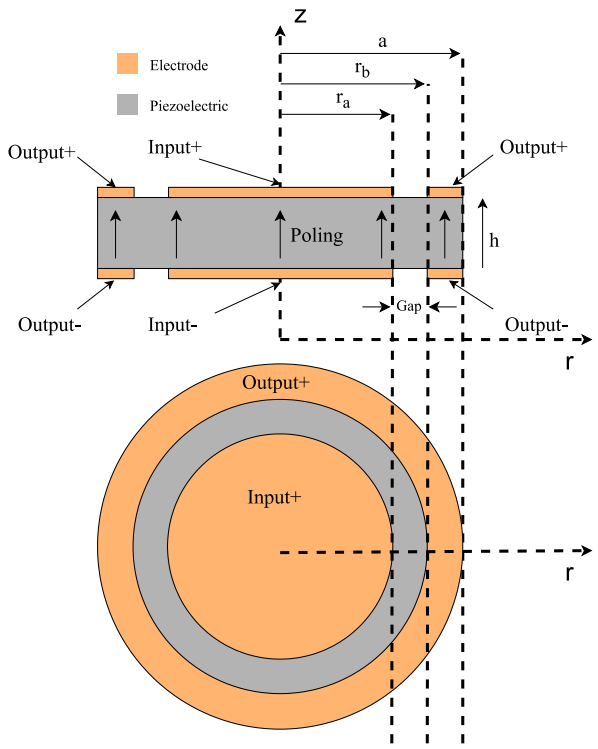

Fig. 2. Cross-section and top-down view of Ring-Dot PT

The model derived here is obtained from a 1D (radial axis) analysis of a ring-dot device, operating exclusively with radial motion. Whilst this is a 1D analysis, the device being analysed has a finite thickness; however, we will assume all parameters (such as stress, strain, and electric field) are constant across the thickness of the device. Additionally, the PT's finite thickness is captured by the model using the material density. A diagram of this device is shown in Fig. 2. The PT is made of a single disc of piezoelectric material, with a ring-dot electrode on both top and bottom faces. It is assumed that the positive electrodes are on the top face of the PT (shown in Fig. 2), with the top dot electrode as the positive input and the top ring electrode as the positive output. The bottom dot and ring electrodes provide the negative input and output connections respectively and are physically and galvanically isolated from each other. The electrodes are assumed to be made of a highly conductive material (copper, platinum, gold) with negligible thickness and so do not affect the vibration behaviour of the PT.

The PT is split into 3 regions, dot (input), inner-ring (gap) and outer-ring (output), as shown in Fig. 3. Fig. 3 also illustrates the cylindrical coordinate system and PT dimensions used throughout this paper with the PT thickness, T, in the z axis and the disc and electrode radii along the r axis. Each section will be analysed separately based on the forces and velocities acting on it, thus allowing an equivalent circuit to be generated for each section. Then, all the three equivalent circuits will be combined, noting the forces and velocities are equal on the boundaries of sections. The whole PT equivalent circuit will

then be simplified to the Mason equivalent circuit form, providing equations for each of the electrical components based on the PT geometry and material. This stage is crucial as the circuit form can be used by electrical engineers to design power converters.

We assume that the PT being analysed is polled only in the volume between the top and bottom dot electrodes and the top and bottom ring-electrodes. The non-electroded region of the disc – the 'gap' – will be assumed to be made of unpoled piezoelectric and hence will be assumed to act like an elastic, insulating material with the mechanical properties of the unpolled piezoelectric material.

To facilitate this analysis, it will be assumed that the PT follows Kirchhoff's thin-plate theory (CPT), which is well-discussed in [24]–[26]. The implications of these assumptions are as follows: firstly, it is assumed that the PT is in perfect axisymmetric motion, and hence shear stress and strain are negligible. The PT is assumed to be thin with the radius much greater than thickness ($a \gg h$), therefore stress T_z is negligible. Additionally, electric fields, other than in the thickness (z) direction will be assumed to be negligible.

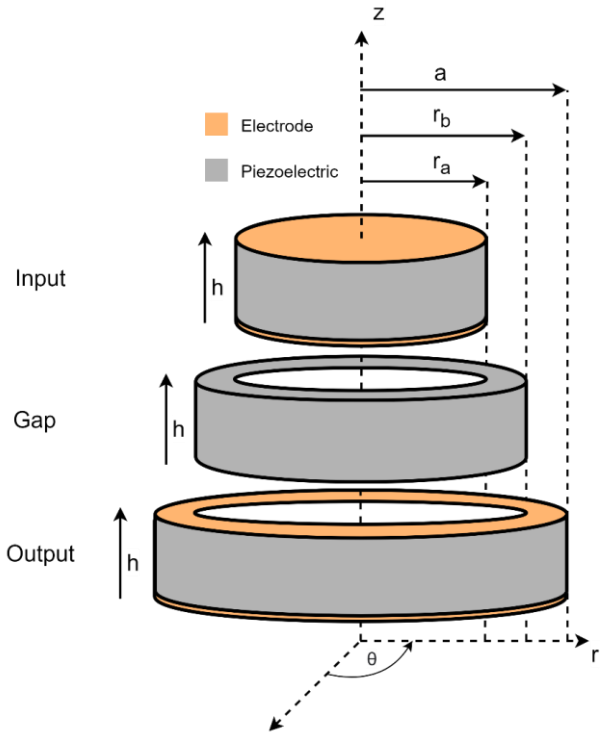

Fig. 3. Ring-dot PT expanded into 3 distinct sections

III. Derivation

The derivation will be handled in 3 separate parts for each of the sections of the device. For each section, an equation for the radial displacement along its length will be found. Using these equations, the electrical and mechanical properties of each section will be evaluated, allowing equations for the force on the outer and inner edges of the section to be found, along with the current flowing into/out of each section's electrodes. Based on the equations for force and current, equivalent circuits will be found for each section.

A. *Foundation Equations*

The constitutive equations for a piezoelectric disc polled in the 'z' direction from CPT are given by [27]

$$T_{r_{\mathrm{in,out,gap}}}(r) = \frac{S_{r_{\mathrm{in,out,gap}}} + \sigma S_{\theta_{\mathrm{in,out,gap}}}}{(s_{11}^{\mathrm{E}}(1-\sigma^2))} - \frac{d_{31}E_{z_{\mathrm{in,out,gap}}}}{s_{11}^{\mathrm{E}}(1-\sigma)} \quad (1)$$

$$T_{\theta_{\mathrm{in,out,gap}}}(\mathrm{r}) = \frac{S_{\theta_{in,out,gap}} + \sigma S_{r_{in,out,gap}}}{(s_{11}^{\mathrm{E}}(1-\sigma^2))} - \frac{d_{31}E_{z_{in,out,gap}}}{s_{11}^{\mathrm{E}}(1-\sigma)} \quad (2)$$

$$D_{z_{\mathrm{in,out,gap}}}(\mathrm{r}) = d_{31}\left(T_{r_{\mathrm{in,out,gap}}} + T_{\theta_{\mathrm{in,out,gap}}}\right) + \varepsilon_{33}^{\mathrm{T}}E_{z_{\mathrm{in,out,gap}}} \quad (3)$$

where $T_{r,\theta}$ is the stress in the r,θ axis and the subscript '$_{\mathrm{in,out,gap}}$' denotes either in or out or gap, as the case may be, depending on the section being analysed, $S_{r,\theta}$ is the strain, D_z is the electric displacement, d_{31} is the piezoelectric strain constant, s_{11}^{E} is the elastic compliance in the radial direction, $\varepsilon_{33}^{\mathrm{T}}$ is the dielectric constant in the thickness direction and σ is Poisson's ratio given by

$$\sigma = -\frac{s_{12}^{\mathrm{E}}}{s_{11}^{\mathrm{E}}} \quad (4)$$

Electric fields $E_{z_{\mathrm{in,out,gap}}}$ in the respective regions are,

$$E_{z_{\mathrm{in}}} = \frac{V_{\mathrm{in}}}{h}, E_{z_{\mathrm{out}}} = \frac{V_{\mathrm{out}}}{h}, E_{z_{\mathrm{gap}}} = 0 \quad (5)$$

From the previous assumptions and assuming perfect axisymmetric motion, strains in the radial (r) and azimuth (θ) direction are given by,

$$S_r = \frac{\partial u_{r_{\mathrm{in,out,gap}}}(r)}{\partial r} \quad (6)$$

$$S_\theta = \frac{u_{r_{\mathrm{in,out,gap}}}(r)}{r} \quad (7)$$

where u_r is radial displacement and r is the radial co-ordinate. Finally, the equation of radial motion in each of the sections of the thin disc [27] is given by,

$$\frac{\partial T_{r_{\mathrm{in,out,gap}}}}{\partial r} + \frac{T_{r_{\mathrm{in,out,gap}}} - T_{\theta_{\mathrm{in,out,gap}}}}{r} = -\rho\omega^2 u_{r_{\mathrm{in,out,gap}}} \quad (8)$$

where ω is the frequency of harmonic radial motion (rad s^{-1}) and ρ is the density of the piezoelectric material. Solving the equation of radial motion (8) for radial displacement, assuming harmonic excitation, gives,

$$u_{r_{\mathrm{in,out,gap}}}(r,t) = \left[C1_{\mathrm{in,out,gap}}\,\mathrm{J}_1(\beta r) + C2_{\mathrm{in,out,gap}}\,\mathrm{Y}_1(\beta r)\right]e^{j\omega t} \quad (9)$$

where $C1, C2$ are constants, J_n and Y_n are n^{th} order Bessel functions of the first and second kind respectively, and β is defined as,

$$\beta = \omega\sqrt{s_{11}^{\mathrm{E}}\rho(1-\sigma^2)} \tag{10}$$

B. Dot – Input section

The dot (input) section will be analysed first since it is the simplest section consider and the methodology used will provide the framework for analysing the remaining two sections. Fig. 4 shows velocity v_1 and force F_1 acting on the outer edge of the dot section of the PT.

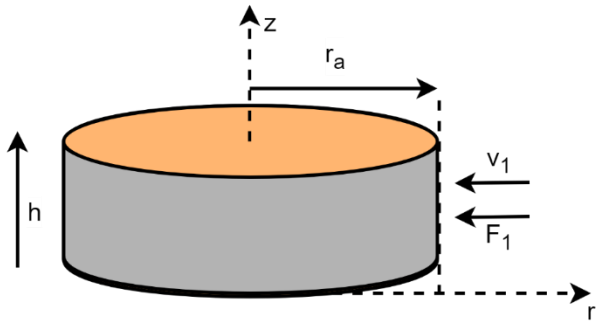

Fig. 4. Dot section, highlighting force acting on the section and velocity on the outer edge

1) Displacement

Constants, $C1_{\text{in}}$and $C2_{\text{in}}$ in (9), are found using the vibration velocity v_1 of the PT. First, noting that at the centre of the disc ($r = 0$), the displacement must be finite, substituting $r = 0$ into (9), it can be shown that $Y_1(r \to 0) \to \infty$. As a result, $C2_{\text{in}} = 0$. $C1_{\text{in}}$ can then be found by first finding the velocity of the outer edge $r = r_a$ of this section. The vibration velocity is found by differentiating with respect to time the radial displacement (9) at the outer edge of the dot section, giving

$$v_1(t) = \frac{\partial u_r(r_a)}{\partial t} = -\mathrm{j}\omega C1_{\text{in}}\mathrm{J}_1(\beta r_a)e^{\mathrm{j}\omega t} \tag{11}$$

where $\mathrm{j} = \sqrt{-1}$. Note that the minus sign in (11) is due to the direction of velocity being defined opposite to the radial coordinate. Therefore, $C1_{\text{in}}$ is given by

$$C1_{\text{in}} = \frac{\mathrm{j}v_1(t)}{\mathrm{J}_1(\beta r_a)\omega e^{\mathrm{j}\omega t}} \tag{12}$$

Finally, substituting (12) and $C2_{\text{in}} = 0$ into (9) gives the displacement of a point in the dot section,

$$u_{r_{\text{in}}}(r,t) = v_1(t)\frac{\mathrm{j}}{\omega}\frac{\mathrm{J}_1(\beta r)}{\mathrm{J}_1(\beta r_a)} \tag{13}$$

2) Electrical Equations

Equations for the current flowing into the input section will now be derived. The charge on the input dot electrode, Q_{in} is given by Gauss's law in terms of electric displacement, D_z,

$$Q_{\text{in}} = 2\pi\int_0^{r_a}\left[D_{z_{\text{in}}}r\right]dr \tag{14}$$

Substituting equations (1)-(3) and (6)-(7) into (14), and with some manipulation, gives

$$Q_{\text{in}} = \frac{-2\pi}{(1-\sigma)s_{11}^{\mathrm{E}}}\int_0^{r_a}\left[d_{31}\left(-\frac{\partial u_{r_{\text{in}}}}{\partial r}r - u_{r_{\text{in}}}\right) + \left(2{d_{31}}^2 - s_{11}^{\mathrm{E}}\varepsilon_{33}^{\mathrm{T}}(1-\sigma)\right)E_{z_{\text{in}}}r\right]dr \tag{15}$$

The current into the dot electrode I_{in}, is given by,

$$I_{\text{in}} = \frac{\partial Q_{\text{in}}}{\partial t} = \mathrm{j}\omega Q_{\text{in}} \tag{16}$$

assuming harmonic excitation, $Q_{\text{in}} = Q_{\text{in}_0}e^{\mathrm{j}\omega t}$. Substituting (15) into (16), with (5) and (13) gives an equation for the magnitude of the input current,

$$I_{\text{in}} = \frac{\mathrm{j}\omega r_a^2\pi\left(2d_{31}^2 + s_{11}^{\mathrm{E}}\varepsilon_{33}^{\mathrm{T}}(\sigma-1)\right)}{h(\sigma-1)s_{11}^{\mathrm{E}}}V_{\text{in}} - \frac{(2r_a\pi d_{31})}{(\sigma-1)s_{11}^{\mathrm{E}}}v_1 \tag{17}$$

where h is the thickness of the disc. As in [28], a force factor A_{in} can be defined. The force factor describes the conversion from mechanical to electrical energy (or from electrical to mechanical with respect to the output force factor A_{out}). The A_{in} force factor is defined as

$$A_{\text{in}} = -\frac{2r_a\pi d_{31}}{(1-\sigma)s_{11}^{\mathrm{E}}} \tag{18}$$

noting that A_{in} has been written to emphasise that it is negative. Using A_{in}, (17) can be further simplified to

$$I_{\text{in}} = \mathrm{j}\omega C_{\text{in}}V_{\text{in}} - A_{\text{in}}v_1 \tag{19}$$

where the input capacitance, C_{in}, is given by

$$C_{\text{in}} = \frac{r_a^2\pi\left(2d_{31}^2 + s_{11}^{\mathrm{E}}\varepsilon_{33}^{\mathrm{T}}(\sigma-1)\right)}{h(\sigma-1)s_{11}^{\mathrm{E}}} = \frac{r_a^2\pi\varepsilon_{33}^{\mathrm{T}}}{h}(1-k_p^2) \tag{20}$$

and k_p is given by

$$\mathrm{k_p} = \sqrt{2}\sqrt{\frac{d_{31}^2}{\left(e_{33}S_{11}(1-\sigma)\right)}} \tag{21}$$

3) Mechanical Equations

Observing Fig. 4, the force F_1 acts inwards on the outer edge of the dot section. This force is given by,

$$F_1 = \text{Area}\cdot\text{Stress} = [-2\pi hr_a]T_{r_{\text{in}}}(r_a) \tag{22}$$

again, noting the minus sign in (22) as the force is defined in the opposite direction to the r coordinate. Substituting (1), (5)-(7) in to (22) gives

$$F_1 = -\frac{2\pi r_a h}{s_{11}^{\mathrm{E}}(1-\sigma^2)}\left(\frac{\partial u_{r\mathrm{in}}}{\partial r}+\frac{\sigma u_{r\mathrm{in}}}{r} - \frac{d_{31}V_{\mathrm{in}}(1+\sigma)}{h}\right) \quad (23)$$

Substituting (13) into (23) and using $\frac{d}{dx}\mathrm{J}_n(x) = \frac{n}{x}\mathrm{J}_n(x) - \mathrm{J}_{n+1}(x)$ gives (26). Finally, using the previously defined A_{in} force factor (18), equation (26) can be simplified to,

$$F_1 = A_{\mathrm{in}}V_{\mathrm{in}} + v_1 Z_a \quad (24)$$

where the impedance Z_a is defined as

$$Z_a = \frac{2\pi \mathrm{j}h}{s_{11}^{\mathrm{E}}(\sigma^2-1)\omega} \cdot \frac{\left((\sigma-1)\mathrm{J}_1(\beta r_a)+\mathrm{J}_0(\beta r_a)r_a\beta\right)}{\mathrm{J}_1(\beta r_a)} \quad (25)$$

4) Equivalent circuit

Based on (19) and (24), and treating force in an analogous way to voltage and velocity in an analogous way to current, an equivalent circuit can be generated. Horsley *et al* [28], showed that A_{in} can be modelled as an ideal transformer. Fig. 5 shows the equivalent circuit for the input dot section of the ring-dot PT.

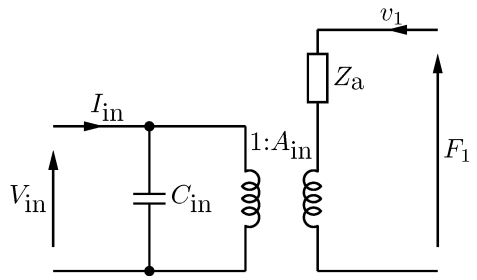

Fig. 5. Equivalent circuit for the dot section of the PT

C. Inactive (gap) ring section

The inactive ring is the section of the PT without electrodes and is the gap between the input and output sections of the PT. Fig. 6 shows vibration velocities, v_{1g} and v_{2g}, and forces, F_{1g} and F_{2g}, acting on the inner and outer edges of the inactive ring section of the PT.

It should be noted that $F_{1g} = -F_1$ and $v_{1g} = -v_1$, however, initially we will assume that these forces and velocities are independent in each section.

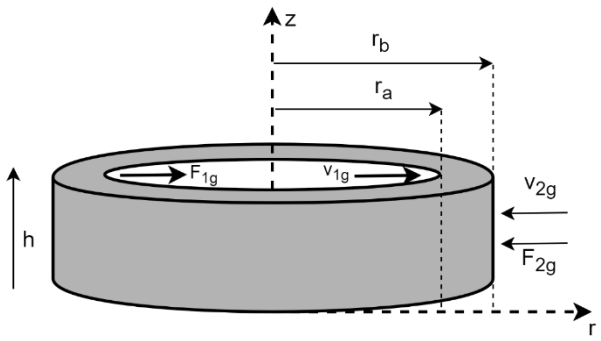

Fig. 6. Forces and velocities acting on the inner-ring section of the PT

1) Displacement

Again, starting from the general solution to the equation of motion (9), constants $C1_{\mathrm{gap}}$ and $C2_{\mathrm{gap}}$ are found using the vibration velocities, v_{1g} and v_{2g}. Observing Fig. 6, the vibration velocity acting on the inner edge, v_{1g}, can be found by differentiating the radial displacement at the inner edge (9) with respect to time, giving

$$v_{1g}(t) = \frac{\partial u_r(r_a)}{\partial t} \quad (28)$$

$$v_{1g}(t) = \mathrm{j}\omega\left(C1_{\mathrm{gap}}\mathrm{J}_1(\beta r_a) + C2_{\mathrm{gap}}\mathrm{Y}_1(\beta r_a)\right)e^{\mathrm{j}\omega t} \quad (29)$$

Similarly, vibration velocity on the outer edge, v_{2g}, can be found by differentiating the radial displacement at the outer edge (9), giving

$$v_{2g}(t) = -\frac{\partial u_r(r_b)}{\partial t} \quad (30)$$

$$v_{2g}(t) = -\mathrm{j}\omega\left(C1_{\mathrm{gap}}\mathrm{J}_1(\beta r_b) + C2_{\mathrm{gap}}\mathrm{Y}_1(\beta r_b)\right)e^{\mathrm{j}\omega t} \quad (31)$$

Again, note the minus sign in (31) due to v_{2g} being defined in the opposite direction to the r coordinate. As both (29) and (31) contain two unknowns, they will be solved simultaneously. Rearranging (29) and (31) for $C2_{\mathrm{gap}}$ gives

$$C2_{\mathrm{gap}} = \frac{-\mathrm{J}_1(\beta r_a)C1_{\mathrm{gap}}\omega - \mathrm{j}e^{\mathrm{j}\omega t}v_{1g}}{Y_1(\beta r_a)\omega} \quad (32)$$

$$F_1 = -\frac{2\pi r_a h\left(-\frac{d_{31}V_{in}(1+\sigma)}{h}+\frac{v_1\left(J_0(r\beta)r\beta+\sigma J_1(r\beta)-J_1(r\beta)\right)j}{J_1(\beta r_a)r\omega}\right)}{s_{11}^{E}(-\sigma^2+1)} \quad (26)$$

$$u_{r_{\mathrm{gap}}}(r,t) = \frac{\mathrm{j}}{\omega}\frac{\mathrm{J}_1(\beta r_a)\mathrm{Y}_1(\beta r)v_{2g} + \mathrm{J}_1(\beta r_b)\mathrm{Y}_1(\beta r)v_{1g} - \mathrm{J}_1(\beta r)\mathrm{Y}_1(\beta r_b)v_{1g} - \mathrm{J}_1(\beta r)\mathrm{Y}_1(\beta r_a)v_{2g}}{\mathrm{J}_1(\beta r_a)\mathrm{Y}_1(\beta r_b) - \mathrm{Y}_1(\beta r_a)\mathrm{J}_1(\beta r_b)} \quad (27)$$

$$C2_{\text{gap}} = \frac{-\mathrm{J}_1(\beta r_b)C1_{\text{gap}}\omega + \mathrm{j}e^{\mathrm{j}\omega t}v_{2g}}{Y_1(\beta r_b)\omega} \quad (33)$$

Equating (32) and (33), and solving for $C1_{\text{gap}}$ gives,

$$C1_{\text{gap}} = \frac{\mathrm{j}\left(v_{1g}\mathrm{Y}_1(\beta r_b) + v_{2g}\mathrm{Y}_1(\beta r_a)\right)e^{-\mathrm{j}\omega t}}{\omega\left(\mathrm{J}_1(\beta r_a)\mathrm{Y}_1(\beta r_b) - \mathrm{Y}_1(\beta r_a)\mathrm{J}_1(\beta r_b)\right)} \quad (34)$$

$C2_{\text{gap}}$ is then found by substituting (34) into either (32) or (33) and simplifying, giving,

$$C2_{\text{gap}} = \frac{\mathrm{j}\left(v_{1g}\mathrm{J}_1(\beta r_b) + v_{2g}\mathrm{J}_1(\beta r_a)\right)e^{-\mathrm{j}\omega t}}{\omega\left(\mathrm{J}_1(\beta r_a)\mathrm{Y}_1(\beta r_b) - \mathrm{Y}_1(\beta r_a)\mathrm{J}_1(\beta r_b)\right)} \quad (35)$$

Finally, substituting (34) and (35) into the general equation for radial displacement in (9), gives an equation for the displacement of a particle in the gap section of the device (27).

2) Electrical Equations

As there is no electrode in this section of the device, the external electric field across the thickness of the gap region is ~0. To simplify the derivation of the equivalent circuit of the gap section it is assumed that the electric field through the thickness of the device is zero ($E_{z_{gap}} = 0$) and a FEA simulation result will be shown later in the paper to support the validity of this assumption (Fig. 18). It should be noted that if the gap region is made of polled piezoelectric material, other authors have found an electric field is generated across the thickness of the device [29]. To avoid this complexity, the gap region is assumed to be an elastic material with the same mechanical properties as the piezoelectric material and behaves like an electrical insulator. This simplification leads to

$$D_{z_{\text{gap}}} = 0, E_{z_{gap}} = 0 \quad (36)$$

and, by extension,

$$Q_{\text{gap}} = 0, I_{\text{gap}} = 0 \quad (37)$$

3) Mechanical Equations

As seen in Fig. 6, the force F_{1g} acts inwards on the inner radius and F_{2g} acts inwards on the outer radius of the gap section. These forces are given by

$$F_{1g} = -[2\pi h r_a]T_{r_{gap}}(r_a) \quad (38)$$

$$F_{2g} = -[2\pi h r_b]T_{r_{\text{gap}}}(r_b) \quad (39)$$

Substituting (1) into (38) and (39), using (36) and (37), and the equation for the radial displacement in the inactive inner ring (27), this gives equations for the forces F_{1g} and F_{2g},

$$F_{1g} = Z_1 v_{1g} + Z_2 v_{2g} \quad (40)$$

$$F_{2g} = Z_2 v_{1g} + Z_3 v_{2g} \quad (41)$$

where impedances $Z_{1,2,3}$ are defined in (42) - (44), where x and y are given by,

$$\begin{aligned} Z_1 = \frac{y\pi}{x}[&(\sigma - 1)\mathrm{Y}_1(\beta r_a) \\ &+ r_a\mathrm{Y}_0(\beta r_a)\beta]\mathrm{J}_1(\beta r_b) \\ &- \mathrm{Y}_1(\beta r_b)[(\sigma - 1)\mathrm{J}_1(\beta r_a) \\ &+ \mathrm{J}_0(\beta r_a)r_a\beta] \end{aligned} \quad (42)$$

$$Z_2 = \frac{2y}{x} \quad (43)$$

$$\begin{aligned} Z_3 = \frac{y\pi}{x}[&(\sigma - 1)\mathrm{Y}_1(\beta r_b) \\ &+ r_b\mathrm{Y}_0(\beta r_b)\beta]\mathrm{J}_1(\beta r_a) \\ &- \mathrm{Y}_1(\beta r_a)[(\sigma - 1)\mathrm{J}_1(\beta r_b) \\ &+ \mathrm{J}_0(\beta r_b)r_b\beta] \end{aligned} \quad (44)$$

$$\begin{aligned} x &= \mathrm{J}_1(\beta r_a)\mathrm{Y}_1(\beta r_b) - \mathrm{Y}_1(\beta r_a)\mathrm{J}_1(\beta r_b), \\ y &= \frac{2\mathrm{j}h}{s_{11}^{\mathrm{E}}\omega(\sigma^2 - 1)} \end{aligned} \quad (45)$$

4) Equivalent circuit

In a similar manner to the dot section, an equivalent circuit can be created based on equations for the two forces, F_{1g} and F_{2g}. An equivalent circuit for the inactive inner ring is shown in Fig. 7.

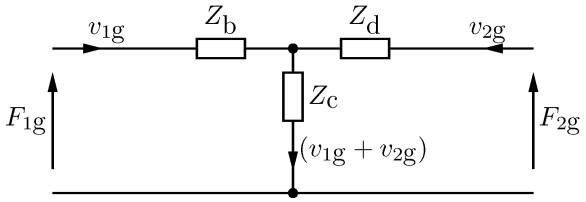

Fig. 7. Combined equivalent circuit for the inactive inner-ring section of the ring-dot PT

where impedances $Z_{b,c,d}$ are defined as,

$$\begin{aligned} Z_b = Z_1 - Z_2 = \frac{y}{x}[&(\sigma - 1)\mathrm{Y}_1(\beta r_a) \\ &+ r_a\mathrm{Y}_0(\beta r_a)\beta]\pi\mathrm{J}_1(\beta r_b) - 2 \\ &- \pi[(\sigma - 1)\mathrm{J}_1(\beta r_a) \\ &+ \mathrm{J}_0(\beta r_a)r_a\beta]\mathrm{Y}_1(\beta r_b) \end{aligned} \quad (46)$$

$$Z_c = Z_2 = \frac{2y}{x} \quad (47)$$

$$\begin{aligned} Z_d = Z_3 - Z_2 = \frac{y}{x}\pi[&(\sigma - 1)\mathrm{Y}_1(\beta r_b) \\ &+ r_b\mathrm{Y}_0(\beta r_b)\beta]\mathrm{J}_1(\beta r_a) - 2 \\ &- \pi[(\sigma - 1)\mathrm{J}_1(\beta r_b) \\ &+ \mathrm{J}_0(\beta r_b)r_b\beta]\mathrm{Y}_1(\beta r_a) \end{aligned} \quad (48)$$

D. Outer ring - Output

The velocity and forces acting on the inner and outer edges of the outer-ring section of the PT are shown in Fig. 8.

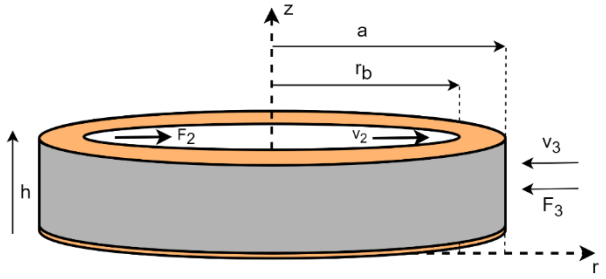

Fig. 8. Forces and velocities acting on the outer-ring section of the ring-dot PT

From the general solution of the equation of motion (9), constants $C1_{\text{out}}$ and $C2_{\text{out}}$ are again found using the vibration velocities v_2 and v_3. Observing Fig. 8, the vibration velocity acting on the inner edge, v_2, is given by

$$v_2(t) = \frac{\partial u_{r_{\text{out}}}(r_b)}{\partial t} \tag{49}$$

$$v_2(t) = \mathrm{j}\omega\big(C1_{\text{out}}\mathrm{J}_1(\beta r_b) + C2_{\text{out}}\mathrm{Y}_1(\beta r_b)\big)e^{\mathrm{j}\omega t} \tag{50}$$

Similarly, vibration velocity on the outer edge, v_3, is given by

$$v_3(t) = -\frac{\partial u_{r_{\text{out}}}(a)}{\partial t} \tag{51}$$

$$v_3(t) = -\mathrm{j}\omega\left(C_{1_{\text{out}}}\mathrm{J}_1(\beta a) + C2_{\text{out}}\mathrm{Y}_1(\beta a)\right)e^{\mathrm{j}\omega t} \tag{52}$$

Again, note the minus sign in (52) due to v_{2g} being defined in the opposite direction to the r coordinate. Rearranging both (50) and (52) for $C2_{\text{out}}$ gives

$$C2_{\text{out}} = \frac{-\mathrm{J}_1(\beta r_b)C1_{\text{out}}\omega - \mathrm{j}e^{-\mathrm{j}\omega t}v_2}{\mathrm{Y}_1(\beta r_b)\omega} \tag{53}$$

$$C2_{\text{out}} = \frac{-\mathrm{J}_1(\beta a)C1_{\text{out}}\omega + \mathrm{j}e^{-\mathrm{j}\omega t}v_3}{\mathrm{Y}_1(\beta a)\omega} \tag{54}$$

Then, solving (53) and (54) simultaneously for $C1_{\text{out}}$ gives

$$C1_{\text{out}} = \frac{\mathrm{j}\big(v_2\mathrm{Y}_1(\beta a) + v_3\mathrm{Y}_1(\beta a)\big)e^{-\mathrm{j}\omega t}}{\omega\big(\mathrm{J}_1(\beta a)\mathrm{Y}_1(\beta r_b) - \mathrm{Y}_1(\beta a)\mathrm{J}_1(\beta r_b)\big)} \tag{59}$$

$C2_{\text{out}}$ can then be found by substituting (59) into either (53) or (54) and simplifying to give

$$C2_{\text{out}} = \frac{-\mathrm{j}\big(v_2\mathrm{J}_1(\beta a) + v_3\mathrm{J}_1(\beta r_b)\big)e^{-\mathrm{j}\omega t}}{\omega\big(\mathrm{J}_1(\beta a)\mathrm{Y}_1(\beta r_b) - \mathrm{Y}_1(\beta a)\mathrm{J}_1(\beta r_b)\big)} \tag{60}$$

Finally, substituting (59) and (60) into the general solution for the equation of motion (9), an equation for the displacement of a particle in the outer-ring section of the device is given in (55).

1) Electrical Equations

The charge into the output ring electrode, Q_{out} is given by Gauss's law,

$$Q_{\text{out}} = 2\pi\int_{r_b}^{a}\left[D_{z_{\text{out}}}r\right]\mathrm{d}r \tag{61}$$

Substituting (1)-(3) and (6)-(7) into (61) gives

$$Q_{\text{out}} = \frac{-2\pi}{(1-\sigma)s_{11}^{\mathrm{E}}}\int_{r_b}^{a}\left[d_{31}\left(-\frac{\partial u_{r_{\text{out}}}}{\partial r}r - u_{r_{\text{out}}}\right) + r\begin{pmatrix}2d_{31}^2 \\ +s_{11}^{\mathrm{E}}\varepsilon_{33}^{\mathrm{T}}(\sigma-1)\end{pmatrix}E_{z_{\text{out}}}\right]\mathrm{d}r \tag{62}$$

The current into outer ring electrode is then given by

$$I_{\text{out}} = \frac{\partial Q_{\text{out}}}{\partial t} = \mathrm{j}\omega Q_{\text{out}} \tag{63}$$

assuming harmonic excitation, $Q_{\text{out}} = Q_{\text{out}_0}e^{\mathrm{j}\omega t}$. Substituting (62) into (63), with (5) and (55) gives an equation for the output current,

$$I_{\text{out}} = \frac{\mathrm{j}\pi(a^2 - r_b^2)\left(2d_{31}^2 + s_{11}^{\mathrm{E}}\varepsilon_{33}^{\mathrm{T}}(\sigma-1)\right)\omega}{h(\sigma-1)s_{11}^{\mathrm{E}}}V_{\text{out}} - \frac{2\pi d_{31}}{(1-\sigma)s_{11}^{\mathrm{E}}}(r_b v_2 + a v_3) \tag{64}$$

As with the input dot section, using the A_{out} force factor allows (64) to be further simplified to

---

$$u_{r_{\text{out}}}(\mathrm{r},\mathrm{t}) = \frac{\mathrm{j}(\mathrm{J}_1(\beta r)\mathrm{Y}_1(\beta r_b)v_3 - \mathrm{J}_1(\beta a)\mathrm{Y}_1(\beta r)v_2 - \mathrm{J}_1(\beta r_b)\mathrm{Y}_1(\beta r)v_3 + \mathrm{J}_1(\beta r)\mathrm{Y}_1(\beta a)v_2)}{\big(\mathrm{J}_1(\beta a)\mathrm{Y}_1(\beta r_b) - \mathrm{Y}_1(\beta a)\mathrm{J}_1(\beta r_b)\big)\omega} \tag{55}$$

$$Z_4 = \frac{2\mathrm{j}h\pi}{s_{11}^{\mathrm{E}}(\sigma^2 - 1)\omega}\frac{\Big(\big((\sigma - 1)Y_1(\beta r_b) + r_b Y_0(\beta r_b)\beta\big)J_1(\beta a) - \big((\sigma - 1)J_1(\beta r_b) + J_0(\beta r_b)r_b\beta\big)Y_1(\beta a)\Big)}{Y_1(\beta a)J_1(\beta r_b) - Y_1(\beta r_b)J_1(\beta a)} \tag{56}$$

$$Z_5 = \frac{4\mathrm{j}h}{s_{11}^{\mathrm{E}}\omega(\sigma^2 - 1)}\frac{1}{Y_1(\beta a)J_1(\beta r_b) - Y_1(\beta r_b)J_1(\beta a)} \tag{57}$$

$$Z_6 = \frac{2\mathrm{j}h\pi}{s_{11}^{\mathrm{E}}(\sigma^2 - 1)\omega}\frac{\Big(\big((\sigma - 1)Y_1(\beta a) + aY_0(\beta a)\beta\big)J_1(\beta r_b) - Y_1(\beta r_b)\big((\sigma - 1)J_1(\beta a) + J_0(\beta a)\beta a\big)\Big)}{Y_1(\beta a)J_1(\beta r_b) - Y_1(\beta r_b)J_1(\beta a)} \tag{58}$$

$$I_{\text{out}} = \text{j}\omega C_{\text{out}} V_{\text{out}} - A'_{\text{out}}(r_b v_2 + a v_3) \tag{65}$$

where A'_{out} is defined as

$$A'_{\text{out}} = \frac{2\pi d_{31}}{(1-\sigma)s_{11}^{\text{E}}} \tag{66}$$

and the output capacitance is given by

$$C_{\text{out}} = \frac{\pi(a^2 - r_b^2)\left(2d_{31}^2 + s_{11}^{\text{E}}\varepsilon_{33}^{\text{T}}(\sigma-1)\right)}{h(\sigma-1)s_{11}^{\text{E}}} = \frac{\pi\left(a^2 - r_b^2\right)\varepsilon_{33}^{\text{T}}}{h}(1-k_p^2) \tag{67}$$

It is important to note that the definition of A'_{out} in (66) differs from A_{in} in (18) because there are two edges to this section and therefore two velocities, which complicates the definition of A_{out}. This will be revisited in section III-F.

2) Mechanical Equations

Observing Fig. 8, the force F_2 acts inwards on the inner radius and F_3 acts inward on the outer radius of the outer ring section. These forces are given by

$$F_2 = -[2\pi h r_b]T_{r_{\text{out}}}(r_b) \tag{68}$$

$$F_3 = -[2\pi h a]T_{r_{\text{out}}}(a) \tag{69}$$

Substituting (1) into (68) and (69), using (5)-(7) and the equation for the displacement of a particle in the outer ring section (55) gives equations for the forces F_2 and F_3,

$$F_2 = Z_4 v_2 + Z_5 v_3 + A'_{\text{out}} V_{\text{out}} r_b \tag{70}$$

$$F_3 = Z_5 v_2 + Z_6 v_3 + A'_{\text{out}} V_{\text{out}} a \tag{71}$$

where $Z_{4,5,6}$ are given by equations (56)-(58).

3) Equivalent Circuit

Several manipulations to (70), (71) and (65) must be performed before a single equivalent circuit can be drawn. First, similar to [28], [30] we normalise the forces and velocities

$$F_2' = \frac{F_2}{r_b}, F_3' = \frac{F_3}{a}, v_2' = v_2 r_b, v_3' = v_3 a \tag{75}$$

Therefore, (65) can be re-written as

$$I_{\text{out}} = \text{j}\omega C_{\text{out}} V_{\text{out}} - A'_{\text{out}}(v_2' + v_3') \tag{76}$$

and (70) and (71) can be written as

$$F_2' = \frac{Z_4}{r_b^2} v_2' + \frac{Z_5}{r_b a} v_3' + A'_{\text{out}} V_{\text{out}} \tag{77}$$

$$F_3' = \frac{Z_5}{r_b a} v_2' + \frac{Z_6}{a^2} v_3' + A'_{\text{out}} V_{\text{out}} \tag{78}$$

As done in [31], the manipulations defined in (75) can be performed using ideal transformers. After performing a similar transformation to that used for the inactive gap section, a single equivalent circuit can be formed based on the forces in (77) and (78), as is shown in Fig. 10.

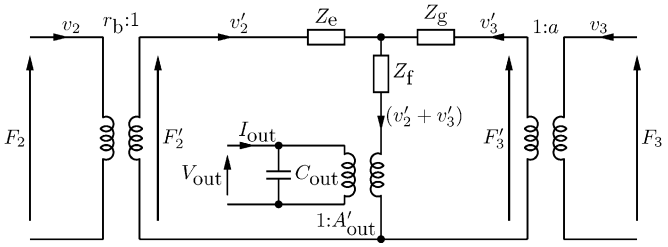

Fig. 10. Equivalent circuit for the outer ring section of the ring-dot PT

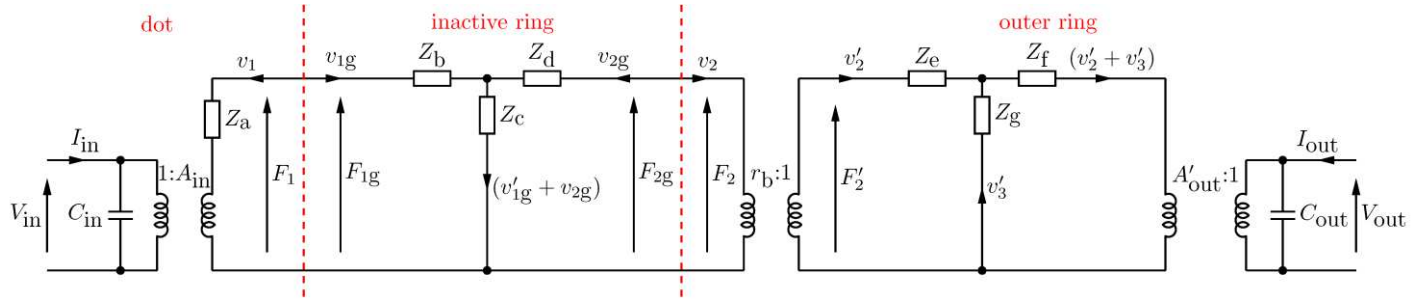

Fig. 9. Full equivalent circuit for the ring-dot PT with $F_3 = 0$

$$Z_e = \frac{Z_4}{r_b^2} - \frac{Z_5}{r_b a} = \frac{2\text{j}h}{s_{11}^{\text{E}}\omega(\sigma^2-1)r_b^2 a} \frac{\begin{pmatrix} a\pi[(\sigma-1)\text{Y}_1(\beta r_b) + r_b \text{Y}_0(\beta r_b)\beta]\text{J}_1(\beta a) \\ -a\pi[(\sigma-1)\text{J}_1(\beta r_b) + \text{J}_0(\beta r_b) r_b \beta]\text{Y}_1(\beta a) - 2r_b \end{pmatrix}}{\text{Y}_1(\beta a)\text{J}_1(\beta r_b) - \text{Y}_1(\beta r_b)\text{J}_1(\beta a)} \tag{72}$$

$$Z_f = \frac{Z_5}{r_b a} = \frac{4\text{j}h}{s_{11}^{\text{E}}\omega(\sigma^2 - 1) r_b a} \frac{1}{\text{Y}_1(\beta a)\text{J}_1(\beta r_b) - \text{Y}_1(\beta r_b)\text{J}_1(\beta a)} \tag{73}$$

$$Z_g = \frac{Z_6}{a^2} - \frac{Z_5}{r_b a} = \frac{2\text{j}h}{s_{11}^{\text{E}}\omega(\sigma^2-1)a^2 r_b} \frac{\begin{pmatrix} r_b\pi[(\sigma-1)\text{Y}_1(\beta a) + a\text{Y}_0(\beta a)\beta]\text{J}_1(\beta r_b) \\ -r_b\pi[(\sigma-1)\text{J}_1(\beta a) + \text{J}_0(\beta a)\beta a]\text{Y}_1(\beta r_b) - 2a \end{pmatrix}}{\text{Y}_1(\beta a)\text{J}_1(\beta r_b) - \text{Y}_1(\beta r_b)\text{J}_1(\beta a)} \tag{74}$$

The transformed impedances $Z_{e,f,g}$ are defined as (72)-(74).

E. Full PT equivalent circuit

Assuming the forces and velocities at the boundaries between sections are equal (i.e. $F_1 = F_{1g}, F_{2g} = F_2, v_1 = -v_{1g}, v_{2g} = -v_2$), the three equivalent circuits can be combined into a single circuit. It is assumed the PT is free to vibrate (free vibration boundary condition), thus the force on the outer edge of the PT, F_3, is 0. Applying this condition and simplifying gives the circuit shown in Fig. 9.

F. Lumped equivalent circuit

The full equivalent circuit in Fig. 9 can now be simplified using several π-to-T and T-to-π circuit transformations, some manipulation and the Bessel function identity [31] given in equation (79).

$$-\frac{2}{\pi} = X\big(\mathrm{J}_0(X)\mathrm{Y}_1(X) - \mathrm{J}_1(X)\mathrm{Y}_0(X)\big) \tag{79}$$

The full simplification process is derived in detail in the Appendix. The resulting simplified equivalent circuit is shown in Fig. 11,

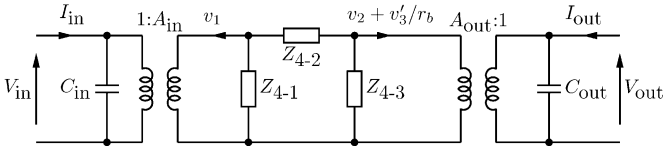

Fig. 11. Simplified the ring-dot equivalent circuit

where impedances $Z_{4\text{-}1}$, $Z_{4\text{-}2}$ and $Z_{4\text{-}3}$ are defined in terms of the impedances $Z_{a\text{-}g}$ and given in (80)-(82).

$$Z_{4\text{-}1} = \frac{\begin{pmatrix}\big[Z_g r_b^2\gamma + (Z_c+\lambda)\gamma - Z_c^2\big]Z_f \\ -Z_g[(-Z_c-\lambda)\gamma + Z_c^2]\end{pmatrix}}{Z_g\lambda + Z_f\big(Z_g r_b^2 + Z_c + \lambda\big)} \tag{80}$$

$$Z_{4\text{-}2} = \frac{\begin{pmatrix}\big[(Z_f+Z_g)Z_c + (Z_f r_b^2 + \lambda)Z_g + Z_f\lambda\big]\gamma \\ -Z_c^2\big[Z_f + Z_g\big]\end{pmatrix}}{Z_g Z_c} \tag{81}$$

$$Z_{4\text{-}3} = \frac{\begin{pmatrix}\begin{bmatrix}(-Z_f - Z_g)Z_c \\ +(-Z_f r_b^2 - \lambda)Z_g - Z_f\lambda\end{bmatrix}\gamma \\ +Z_c^2\big[Z_f + Z_g\big]\end{pmatrix} r_b^2}{(-Z_g r_b^2 - Z_c - \lambda)\gamma + Z_c\big(Z_g r_b^2 + Z_c\big)} \tag{82}$$

and λ and γ are defined as

$$\gamma = Z_a + Z_b + Z_c \tag{83}$$

$$\lambda = Z_e r_b^2 + Z_d \tag{84}$$

And A_{out} is given by

$$A_{\text{out}} = A'_{\text{out}} r_b \tag{85}$$

Substituting impedances Z_{a-g} ((25), (46)-(48), (72)-(74)) into (80)-(82) with (83) and (84) gives the full expressions for $Z_{4\text{-}1,2,3}$ in terms of material and geometrical parameters. The resulting equations have been omitted due to length but are trivial to derive. The equivalent circuit shown in Fig. 11 is now in a suitable format to be simulated using mathematical software tools. However, in this form the equivalent circuit is incompatible for use in circuit-based software tools such as SPICE since each impedance is defined in terms of Bessel functions and not modelled using traditional electrical components.

G. Simplification to the Mason equivalent circuit

In this section, the circuit in Fig. 11 will be further simplified to the Mason equivalent form, which can then be simulated and emulated using traditional electronic components.

1) Finding resonant frequencies

Observing the circuit in Fig. 11, the short circuit resonant frequency of the PT occurs when the numerators of the three impedances are equal to zero ($Z_{4\text{-}1} = Z_{4\text{-}2} = Z_{4\text{-}3} = 0$). Solving the numerators of (80)-(82) equal to zero leads to the following equation,

$$\frac{\mathrm{J}_0(\beta a)\beta a}{\mathrm{J}_1(\beta a)} = \frac{\mathrm{J}_0(R)R}{\mathrm{J}_1(R)} = 1 - \sigma \tag{86}$$

where $\beta a = R$ is the first positive solution of (86). Since equation (86) is defined by Bessel functions it is transcendental and must be solved numerically. Using the first positive solution of R, the first radial resonant frequency of the PT can be found using

$$\omega_0 = \frac{R}{\sqrt{s_{11}^{\mathrm{E}}\rho(1-\sigma^2)\,a}} \tag{87}$$

This agrees with the results reported by Horsley [28] for the radial mode Transoner PT. It is also notable that the resonant frequency is controlled exclusively by the outer radius of the device, and not by the internal radii.

2) Lumped equivalent circuit

To simplify the circuit in Fig. 11 to the traditional lumped Mason equivalent form, an approximation method will be used. First, a Taylor expansion of each impedance in Fig. 11 will be performed around the first radial resonance. The first two terms in the Taylor series for each impedance are

$$Z_{T4\text{-}1} \approx 0 + \frac{\chi}{\mathrm{J}_1\left(\frac{Rr_1}{a}\right)\tau R^2\left(r_2\mathrm{J}_1\left(\frac{Rr_1}{a}\right) + \psi\right)} \tag{88}$$

$$Z_{T4\text{-}2} \approx 0 - \frac{\chi}{R^2\psi\tau\mathrm{J}_1\left(\frac{Rr_1}{a}\right)} \tag{89}$$

$$Z_{T4\text{-}3} \approx 0 + \frac{r_2\chi}{R^2\psi\tau\left(r_2\mathrm{J}_1\left(\frac{Rr_1}{a}\right) + \psi\right)} \tag{90}$$

where ψ, τ and χ are defined as,

$$\psi = \mathrm{J}_1(R)a - \mathrm{J}_1\left(\frac{Rr_2}{a}\right)r_2 \tag{91}$$

$$\tau = (\sigma - 1)\mathrm{Y}_1(R) + R\mathrm{Y}_0(R) \tag{92}$$

$$\chi = 4\mathrm{j}\rho r_2 \left(\mathrm{J}_1\left(\frac{Rr_2}{a}\right) r_2 + \psi\right) h(R^2 + \sigma^2 - 1)a \qquad (93)$$

Then, using the circuit transformation in [32] the circuit in Fig. 11, becomes that shown in Fig. 12.

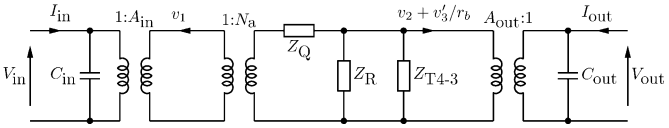

Fig. 12. Simplified ring-dot equivalent circuit after circuit transformation defined in [32] is performed

Where impedances Z_R and Z_Q, and turn ratio N_a are given by

$$Z_R = Z_{T4\text{-}1} + Z_{T4\text{-}2} \qquad (94)$$

$$Z_Q = \frac{Z_{T4\text{-}2}(Z_{T4\text{-}1} + Z_{T4\text{-}2})}{Z_{T4\text{-}1}} \qquad (95)$$

$$N_a = \frac{Z_R}{Z_{T4\text{-}1}} \qquad (96)$$

The circuit in Fig. 12 can then be simplified by first recognising that

$$Z_R + Z_{T4\text{-}3} \to 0 \text{ and } Z_R Z_{T4\text{-}3} \to \infty \qquad (97)$$

Therefore, the parallel combination of Z_R and $Z_{T4\text{-}3}$ tends to ∞, leaving only the Z_Q impedance. Then, the next obvious simplification to the circuit in Fig. 12, would be to combine $1{:}A_{\mathrm{in}}$ and $1{:}N_a$ transformers. However, it is useful to be able to equate the resonant current in the equivalent circuit to the vibration velocity of the PT. While combining A_{in} and N_a would allow that, the resonant current would be equal to $v_2 + v_3'/r_2$ which is not possible to externally measure. Therefore, the remaining impedance, Z_Q, is referred across the $1{:}N_a$ transformer and then the $1{:}N_a$ transformer combines with the $A_{\mathrm{out}}{:}1$. This simplification means the resonant current is equivalent to the vibration velocity, v_1 which is that at the outer edge of the inner-dot section, which is much easier to measure. The resulting circuit is shown in Fig. 13.

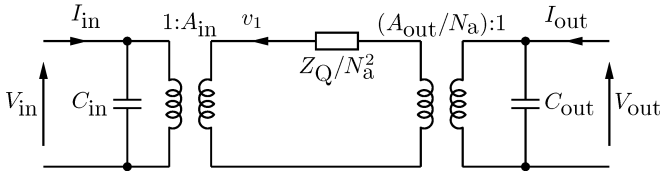

Fig. 13. Simplified ring-dot equivalent circuit

Finally, in order to transform the circuit in Fig. 13 to the Mason equivalent form, the impedance (Z_Q/N_a^2), should be converted to an LC equivalent circuit. First, the impedance of an LC circuit is defined as

$$Z_{\mathrm{eq}} = \mathrm{j}\omega L_m - \frac{\mathrm{j}}{\omega C_m} \qquad (101)$$

where L_m and C_m are the equivalent mechanical inductance and capacitance. Then a Taylor expansion of the equivalent impedance (Z_{eq}) is taken around the resonant frequency of the LC circuit $(\omega_0 = 1/\sqrt{L_m C_m})$, the first two elements of the resulting Taylor series are

$$Z_{T_{\mathrm{eq}}} \approx 0 + 2\mathrm{j}L_m(\omega - \omega_0) \qquad (102)$$

Equating $Z_{T_{\mathrm{eq}}}$ and Z_Q/N_a^2, using (88)-(90), (96) and (95), and solving for L_m gives (98). Then to find C_m, the resonant frequency of the equivalent circuit is used. After substituting in (87) and (98) to $(\omega_0 = 1/\sqrt{L_m C_m})$, and rearranging for C_m gives (99).

3) Damping

In the Mason equivalent circuit model, it is typical to use a resistance in series with the LC circuit to model the losses in the system. The value of this damping resistance is influenced by several factors, including material choice and PT design, but also the physical construction of the device. Therefore, it is difficult to estimate its value. It is common to estimate damping resistance by measuring previous similar devices, made from similar materials. It is also common to define a Q factor for a device, rather than a specific damping resistance, therefore the value of the damping resistance will be defined in terms of the Q factor of the radial mode in a ring-dot device. Firstly, the Q factor of a series RLC circuit is

$$L_m = \frac{2ha^2\rho(R^2 + \sigma^2 - 1)}{R^2} \frac{\mathrm{J}_1(R)}{\left((\sigma - 1)\mathrm{Y}_1(R) + R\mathrm{Y}_0(R)\right)\mathrm{J}_1\left(\frac{Rr_a}{a}\right)^2} \qquad (98)$$

$$C_m = -\frac{s_{11}^{\mathrm{E}}(\sigma^2 - 1)}{2h(R^2 + \sigma^2 - 1)} \frac{\left(R\mathrm{Y}_0(R) + \mathrm{Y}_1(R)\sigma - \mathrm{Y}_1(R)\right)\mathrm{J}_1\left(\frac{Rr_a}{a}\right)^2}{\mathrm{J}_1(R)} \qquad (99)$$

$$R_m = \frac{2}{Q}\sqrt{-\frac{h^2\mathrm{J}_1(R)^2 a^2(R^2 + \sigma^2 - 1)^2\rho}{\left(R\mathrm{Y}_0(R) + \mathrm{Y}_1(R)\sigma - \mathrm{Y}_1(R)\right)^2 R^2 \mathrm{J}_1\left(\frac{Rr_a}{a}\right)^4 s_{11}^{\mathrm{E}}(\sigma^2 - 1)}} \qquad (100)$$

$$Q = \frac{1}{R_m}\sqrt{\frac{L_m}{C_m}} \tag{103}$$

where R_m is the damping resistance. Substituting (98) and (99) into (103) and rearranging for R_m gives (100). Using the newly defined L_m, C_m and R_m, the circuit in Fig. 13 can be simplified to that shown in Fig. 14.

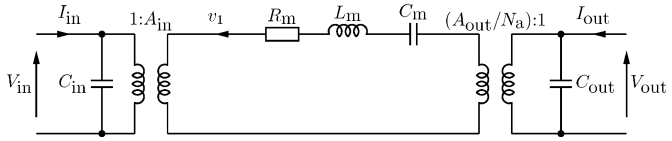

Fig. 14. Ring-dot PT equivalent circuit model transformed to the classic Mason equivalent circuit form

4) Single transformer form

Whilst the circuit in Fig. 13 and accompanying equations allow a ring-dot PT to be simulated and emulated, it is often inconvenient to have two transformers in the circuit. This is because it is difficult to experimentally measure the A_{in} and A_{out} force factors. Unless a direct relationship between the resonant current and the vibration velocity is required, it is more convenient to combine A_{in} and A_{out} transformers into a single transformer, N_1.

To achieve this, first the RLC circuit must be referred across the $1{:}\,A_{in}$ transformer. The resulting RLC components are given by

$$R_1 = R_m/A_{in}^2 \tag{104}$$

$$L_1 = L_m/A_{in}^2 \tag{105}$$

$$C_1 = C_m A_{in}^2 \tag{106}$$

Then combining A_{in}, A_{out} and N_a gives the equivalent turn ratio N_1

$$N_1 = \frac{A_{in}}{\left(\frac{A_{out}}{N_a}\right)} = -\frac{r_a \mathrm{J}_1\left(\frac{Rr_a}{a}\right)}{\mathrm{J}_1(R)a - r_b \mathrm{J}_1\left(\frac{Rr_b}{a}\right)} \tag{107}$$

It is worth noting that the resulting turn ratios from (107) are negative, indicating that the $1{:}N_1$ turn ratio causes a 180° phase shift. The final ring-dot PT equivalent circuit with a single transformer is shown in Fig. 15.

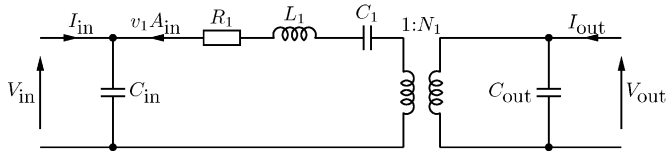

Fig. 15. Single transformer form of the ring-dot PT equivalent circuit

IV. VALIDATION

The validation of the equivalent circuit models will be presented in two parts. Initially, COMSOL will be used to simulate a large number of ideal devices, the equivalent circuit component values extracted and compared to those estimated by the model derived here. Then, the model will be validated against experimental PT data.

A. Representative set of piezoelectric transformers

273 ring-dot PTs were generated by varying r_a, r_b and h over a suitable range. r_a was varied in steps of 0.5mm from $1-7$mm, r_b was varied in steps of 0.5mm from $1.5-7.5$mm and h was varied in steps 0.5mm from $0.5-1.5$mm. It should be noted that only variations where $r_b > r_a + 0.5$mm were allowed. As the radius a determines the resonant frequency (as shown in Equation (87)), its value was kept constant to allow a fixed frequency range to be used for the following FEA simulation.

The PTs were made from PZT-4 material with key parameters given in Table 1. In the inactive section of the PT the same material is used; however, it is treated as an elastic material. Therefore, the PZT in this section acts as an elastic, electrically insulating material.

Table 1 – PZT 4 material properties

$s_{11}^{E}\left(\mathrm{m}^2/\mathrm{N}\right)$	ε_{33}^{T}	$d_{31}\left(\mathrm{m}/\mathrm{V}\right)$	σ	$\rho\left(\mathrm{kg}/\mathrm{m}^3\right)$
1.23×10^{-11}	1300	-1.23×10^{-10}	0.329	7500

B. Comparison to FEA

To get a baseline measurement of the model's accuracy, COMSOL will be used to simulate the representative set of ring-dot PTs. For each PT the equivalent circuit parameters will be estimated using the equivalent circuit model derived here. For this simulation, a 2D axisymmetric model of the ring-dot PT was created and a frequency domain study was used to simulate each device at frequencies between $135-170$kHz, in 10Hz steps. The simulated PT was driven using a 10V sinusoidal signal and the impedance spectra calculated from the resulting currents measured at each frequency. The input section was first driven with the output electrode shorted to the output ground. Then, the output section driven with the input electrode shorted to ground. For all analysis, a free vibration boundary condition was used.

For each PT, $L_1, C_1, C_{in}, C_{out}$ and N_1 were all extracted from the frequency domain COMSOL analysis data using method 3 described [17]. The equivalent circuit values were then estimated using equations (20), (105)-(107). For each PT, the error in the calculated parameter value, compared to the COMSOL simulation result, was calculated. For each parameter, Table 2 shows the mean of the absolute percentage error for each PT (the MAPE), and the standard deviation of the corresponding (signed) percentage errors.

Observing the results in Table 2, the equivalent circuit model very accurately estimates L_1, C_1 and N_1 across the range of tested values, with an average of less than 1% error in each of the three parameters, with a similarly low (<1%) standard deviation in the error. However, estimates of the input and output capacitances show large errors and with a large standard deviation in the results. This result agrees with the findings of Horsley *et al* [28] for the radial mode Transoner PT. Interestingly, removing the piezoelectric element in the equation for these capacitances, gives rise to significant improvements in accuracy as shown in the last two rows of Table 2.

Table 2. Average error and standard deviation in the estimated parameters

Parameter	MAPE (%)	Standard deviation in percentage error (%)
L_1	0.45	0.37
C_1	0.65	0.35
N_1	0.38	0.45
C_{in}	32.3	12.9
C_{out}	30.7	8.1
$C_{\text{in}}/1-k_p^2$	10.4	7.6
$C_{\text{out}}/1-k_p^2$	6.3	5.2

To further confirm the accuracy of the model, the input impedance spectra (with the output terminals shorted) of a sample PT can be extracted from the previous COMSOL simulation and compared to the input impedance estimated by the proposed model. An equation for the input impedance of the PT in terms of equivalent circuit components (with the output terminals shorted) is given by [33],

$$Z_{\text{in}} = \frac{-\text{j} + \omega(\omega L_1 j + R_1)C_1}{\omega\left((C_{\text{in}}R_1\omega\text{j} - C_{\text{in}}L_1\omega^2 + 1)C_1 + C_{\text{in}}\right)} \quad (108)$$

A PT with dimensions, $a = 8\text{mm}$, $r_a = 3\text{mm}$, $r_b = 6\text{mm}$ and $h = 1\text{mm}$ was chosen. Fig. 16 shows the input impedance of the PT extracted from COMSOL, the input impedance predicted by the model using (108) and the input impedance predicted by the model with adjusted $\left(\times \frac{1}{1-k_p^2}\right) C_{\text{in}}$ values.

The results in Fig. 16 show the excellent accuracy of the model around the resonant frequency. At the anti-resonant frequency (impedance maximum), the results from the model show some disparity to those from COMSOL. However, using the adjusted C_{in} value, a significantly more accurate result is achieved.

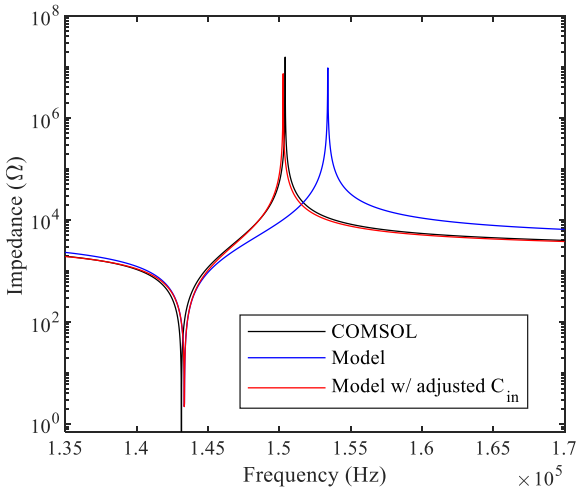

Fig. 16. Input impedance spectra from COMSOL and the model presented here

Another factor influencing the accuracy of the input and output capacitance estimation is the occurrence of an additional parasitic capacitance occurring between the input and output electrodes ($C_{\text{in-to-out}}$), as shown in Fig. 17.

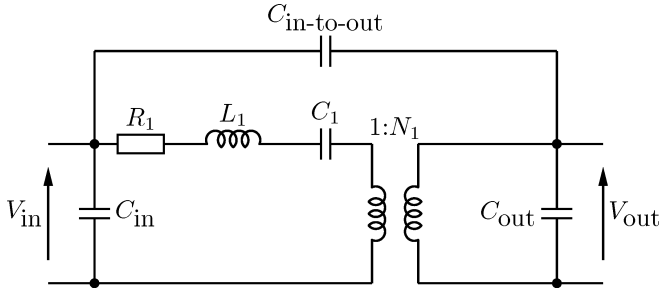

Fig. 17. Single transformer form of the ring-dot PT equivalent circuit with additional parasitic $C_{\text{in-to-out}}$ capacitance

A device with dimensions given in Table 3 was simulated in COMSOL to support the analysis in the paper. Fig. 18 shows the electric field E_z at the intersection of a horizontal line located at $h/2$ extending from $0 < r < a$, during an input impedance measurement with the output connected in short circuit and operating very close to resonance. As is expected, $E_z \approx -10\text{V/mm}$ in the dot section, which is being driven by a 10V source. The output section experiences $E_z \approx 0$, which is to be expected as the output is connected in short circuit. As can be seen E_z transitions within the gap section from -9V/mm to -1V/mm within 1mm. The authors consider this transition to be sufficiently rapid to support the assumption that $E_{z_{gap}} = 0$, for this PT.

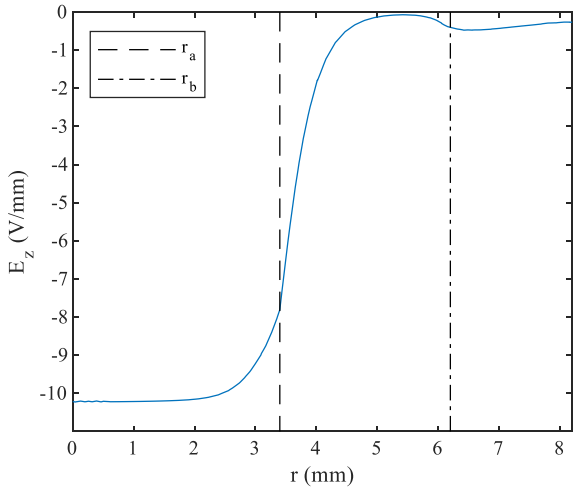

Fig. 18. COMSOL predicted E_z occurring along the radius of the PT (dimensions in Table 3) at $z = h/2$ during input impedance measurement

C. Practical PT validation

The lumped equivalent circuit model derived here is compared to experimental measurement of a practical ring-dot PT.

Fig. 19. PZT based Ring-dot PT

Table 3. Practical device dimensions

r_a(mm)	r_b(mm)	a(mm)	h(mm)
3.4	6.1	8.2	1.1

The device under test is made from PZT-P85 (Weifang Jude Electron) and with dimensions given in Table 3 is shown in Fig. 19. The key material properties for PZT-P85 are shown in Table 4. It should be noted that the PT under test is both a fully poled PT (gap volume is polled) and a 3-electrode device (common electrode stretching across the gap), therefore, contains some minor differences to the PT modelled here.

Table 4. PZT-P85 material properties

s_{11}^{E} $\left(\mathrm{m}^2/\mathrm{N}\right)$	$\varepsilon_{33}^{\mathrm{T}}$	d_{31} $\left(\mathrm{m}/\mathrm{V}\right)$	σ	ρ $\left(\mathrm{kg}/\mathrm{m}^3\right)$	Q
12.0×10^{-12}	1700	-180×10^{-12}	0.30	7600	200

Equations (20), (105)-(107) can be used to estimate the equivalent components of the PT under test. Input and output impedance measurements (with output and input shorted, respectively) are then taken from the PT under test using an Omicron Bode 100 vector network analyser. The equivalent circuit parameters are then extracted from the various impedance measurements using the method presented in [33]. The resulting measured and estimated equivalent circuit components are shown in Table 5.

Observing Table 5, a similar pattern to the FEA results can be observed, with estimated L_1, C_1 and N_1 values showing good accuracy compared to the experimental results. Again, similar to the FEA investigation, C_{in} and C_{out} both show considerable errors compared to experimental results. However, again by removing the effect of the piezoelectric component of the capacitance, the results show significant improvements. Again, additional errors are to be expected in the input and output capacitance, due to not accounting for the parasitic input to output capacitance, which will falsely inflate the experimental input and output capacitance measurements. It should also be noted that, in most cases accurate values of both input and output capacitances are often not required, as accuracy in the estimation of the ratio of input to output capacitance is of much greater importance to PT design [18]. In this example, the percentage error in the input to output capacitance ratio is only 4.3%.

Table 5. Model estimated and experimental values from the ring-dot PT under test

Parameter	Experimental	Model
L_1	16.3mH	14.4mH
C_1	83.4pF	92.1pF
ω_0	137kHz	138kHz
N_1	1.06	1.03
C_{in}	0.54nF	0.24nF
C_{out}	1.45nF	0.63nF
$C_{\mathrm{in}}/1-k_p^2$	-	0.50nF
$C_{\mathrm{out}}/1-k_p^2$	-	1.29nF

V. CONCLUSION

A lumped equivalent circuit model for an electrically isolated ring-dot PT has been derived. This model includes the effect of the 'gap' region that occurs between the input dot and output ring electrodes and presented equations for the lumped equivalent circuit properties. The resulting model is then

validated against COMSOL simulations and experimental PT measurements, showing excellent accuracy in the extracted parameters. This model allows electronic engineers with minimal piezoelectric-specific knowledge to estimate the equivalent circuit properties and subsequently design PTs, lowering the barrier to entry for ring-dot PT based power converters.

VI. Acknowledgements

The authors acknowledge the support from the Engineering and Physical Sciences Research Council under grant EP/S031421/1.

VII. References

[1] M. Ekhtiari, T. G. Zsurzsan, M. A. E. Andersen, and Z. Zhang, 'Optimum Phase Shift in the Self-Oscillating Loop for Piezoelectric-Transformer-Based Power Converters', *IEEE Transactions on Power Electronics*, vol. 33, no. 9, pp. 8101–8109, Sep. 2018, doi: 10.1109/TPEL.2017.2771297.

[2] S. J. Huang, T. S. Lee, and P. Y. Lin, 'Application of Piezoelectric-Transformer-Based Resonant Circuits for AC LED Lighting-Driven Systems With Frequency-Tracking Techniques', *IEEE Transactions on Industrial Electronics*, vol. 61, no. 12, pp. 6700–6709, Dec. 2014, doi: 10.1109/TIE.2014.2320232.

[3] S. Yang, Z. Wu, W. Jia, and G. Wu, 'Ultra-Low Relative Frequency Split Piezoelectric Ring Resonator Designed for High-Performance Mode-Matching Gyroscope', *Journal of Microelectromechanical Systems*, vol. 31, no. 1, pp. 6–8, Feb. 2022, doi: 10.1109/JMEMS.2021.3132371.

[4] L. Wang, K. Sun, and R. Burgos, 'Planar Piezoelectric Transformer-Based High Step-Down Voltage-Ratio DC–DC Converter', *IEEE Transactions on Power Electronics*, vol. 37, no. 9, pp. 10833–10848, Sep. 2022, doi: 10.1109/TPEL.2022.3163427.

[5] M. E. Galanko Klemash *et al.*, '1-Port Piezoelectric Resonators With > 100 V/V Gain', *Journal of Microelectromechanical Systems*, vol. 29, no. 5, pp. 874–880, Oct. 2020, doi: 10.1109/JMEMS.2020.3015229.

[6] Y. Ning, M. Zhang, Y. Lang, Y. Gong, X. Yang, and W. Pang, 'Electronic Stethoscope Based on Triangular Cantilever Piezoelectric Bimorph MEMS Transducers', *Journal of Microelectromechanical Systems*, vol. 31, no. 3, pp. 450–456, Jun. 2022, doi: 10.1109/JMEMS.2022.3160761.

[7] C. Chare, P. Gijsenbergh, Y. Jeong, P. Heremans, D. Cheyns, and J. Genoe, 'Electromechanical Equivalent Circuit Model for Axisymmetric PMUTs With Elastic Boundary Conditions', *Journal of Microelectromechanical Systems*, vol. 31, no. 3, pp. 457–472, Jun. 2022, doi: 10.1109/JMEMS.2022.3151245.

[8] S. Wang, J. Shan, H. Tian, and S. Lin, 'The High-Power Piezoelectric Transformer With Multiple Outputs Based on Sandwiched Piezoelectric Transducers', *IEEE Transactions on Power Electronics*, vol. 37, no. 8, pp. 8886–8894, Aug. 2022, doi: 10.1109/TPEL.2022.3157620.

[9] A. V. Carazo, 'Multilayer piezoelectric transformer', US6614144B2, Sep. 02, 2003 Accessed: Jul. 02, 2018. [Online]. Available: https://patents.google.com/patent/US6614144B2/en#npl Citations

[10] E. L. Horsley, M. P. Foster, and D. A. Stone, 'State-of-the-art Piezoelectric Transformer technology', presented at the 2007 European Conference on Power Electronics and Applications, Sep. 2007. doi: 10.1109/EPE.2007.4417637.

[11] A. Vazquez Carazo and Alfredo, 'Piezoelectric Transformers: An Historical Review', *Actuators*, vol. 5, no. 2, p. 12, Apr. 2016, doi: 10.3390/act5020012.

[12] J. Hans and D. A. Berlincourt, 'Piezoelectric ceramic resonators', US2969512A, Jan. 24, 1961 Accessed: Aug. 25, 2020. [Online]. Available: https://patents.google.com/patent/US2969512/en

[13] J. Erhart, P. Půlpán, R. Dolecek, P. Psota, and V. Lédl, 'Disc Piezoelectric Ceramic Transformers', *IEEE Transactions on Ultrasonics, Ferroelectrics, and Frequency Control*, vol. 60, no. 8, pp. 1612–1618, Aug. 2013, doi: 10.1109/TUFFC.2013.2742.

[14] P. Laoratanakul, A. Vazquez Carazo, P. Bouchilloux, and K. Uchino, 'Unipoled Disk-type Piezoelectric Transformers', *Japanese Journal of Applied Physics*, vol. 41, pp. 1446–1450, Mar. 2002, doi: 10.1143/JJAP.41.1446.

[15] S. Priya, S. Ural, H. W. Kim, K. Uchino, and T. Ezaki, 'Multilayered Unipoled Piezoelectric Transformers', *Jpn. J. Appl. Phys.*, vol. 43, no. 6R, Jun. 2004, doi: 10.1143/JJAP.43.3503.

[16] M. Guo, D. M. Lin, K. H. Lam, S. Wang, H. L. W. Chan, and X. Z. Zhao, 'A lead-free piezoelectric transformer in radial vibration modes', *Review of Scientific Instruments*, vol. 78, no. 3, Mar. 2007, doi: 10.1063/1.2712795.

[17] J. Forrester, J. Davidson, M. Foster, and D. Stone, 'Equivalent Circuit Parameter Extraction Methods for Piezoelectric Transformers', presented at the EPE'19 ECCE Europe, Genoa, Italy, Sep. 2019.

[18] M. P. Foster, J. N. Davidson, E. L. Horsley, and D. A. Stone, 'Critical Design Criterion for Achieving Zero Voltage Switching in Inductorless Half-Bridge-Driven Piezoelectric-Transformer-Based Power Supplies', *IEEE Transactions on Power Electronics*, vol. 31, no. 7, pp. 5057–5066, Jul. 2016, doi: 10.1109/TPEL.2015.2481706.

[19] J. Yang, 'Piezoelectric transformer structural modeling - a review', *IEEE Transactions on Ultrasonics, Ferroelectrics, and Frequency Control*, vol. 54, no. 6, pp. 1154–1170, Jun. 2007, doi: 10.1109/TUFFC.2007.369.

[20] D. J. Falimiaramanana, F. E. Ratolojanahary, J.-E. Lefebvre, L. E. Maimouni, and M. Rguiti, '2-D Modeling of Rosen-Type Piezoelectric Transformer by Means of a Polynomial Approach', *IEEE Transactions on Ultrasonics, Ferroelectrics, and Frequency Control*, vol. 67, no. 8, pp. 1701–1714, Aug. 2020, doi: 10.1109/TUFFC.2020.2975647.

[21] P. Půlpán, J. Erhart, and O. Štípek, 'Analytical Modeling of Piezoelectric Transformers', *Ferroelectrics*, Jun. 2007, doi: 10.1080/00150190701354299.

[22] P. Půlpán and J. Erhart, 'Transformation ratio of "ring-dot" planar piezoelectric transformer', *Sensors and Actuators A: Physical*, vol. 140, no. 2, pp. 215–224, Nov. 2007, doi: 10.1016/j.sna.2007.06.011.

[23] S. Ho, 'Modeling of a Disk-Type Piezoelectric Transformer', *IEEE Transactions on Ultrasonics, Ferroelectrics, and Frequency Control*, vol. 54, no. 10, pp. 2110–2119, Oct. 2007, doi: 10.1109/TUFFC.2007.506.

[24] E. Ventsel and T. Krauthammer, *Thin plates and shells: theory, analysis, and applications*. New York: Marcel Dekker, 2001.

[25] J. N. Reddy, *Theory and analysis of elastic plates*. Philadelphia, PA: Taylor & Francis, 1999.

[26] G. Kirchhoff, 'Ueber die Schwingungen einer kreisförmigen elastischen Scheibe', *Ann. Phys.*, vol. 157, no. 10, pp. 258–264, Jan. 1850, doi: 10.1002/andp.18501571005.

[27] T. Ikeda, *Fundamentals of piezoelectricity*. Oxford ; New York: Oxford University Press, 1990.

[28] E. L. Horsley, A. V. Carazo, M. P. Foster, and D. A. Stone, 'A Lumped Equivalent Circuit Model for the Radial Mode Piezoelectric Transformer', in *2009 Twenty-Fourth Annual IEEE Applied Power Electronics Conference and Exposition*, Feb. 2009, pp. 1747–1753. doi: 10.1109/APEC.2009.4802906.

[29] Q. Wang, S. T. Quek, C. T. Sun, and X. Liu, 'Analysis of piezoelectric coupled circular plate', *Smart Mater. Struct.*, vol. 10, no. 2, 2001, doi: 10.1088/0964-1726/10/2/308.

[30] S. Lin, 'Study on the radial composite piezoelectric ceramic transducer in radial vibration', *Ultrasonics*, vol. 46, no. 1, pp. 51–59, Mar. 2007, doi: 10.1016/j.ultras.2006.10.005.

[31] E. Horsley, 'Modelling and Analysis of Radial Mode Piezoelectric Transformers and Inductor-less Resonant Power Converters', PhD Thesis, University of Sheffield, 2011.

[32] W. P. Mason, *Electromechanical Transducers and Wave Filters*. D. Van Nostrand Company, 1948.

[33] J. Forrester *et al.*, 'Equivalent circuit parameter extraction of low-capacitance high-damping PTs', *Electronics Letters*, Jan. 2020, doi: 10.1049/el.2019.3887.

VIII. APPENDIX

To simplify the equivalent circuit model in Fig. 9 to the traditional Mason equivalent circuit form, several circuit transformations will be used. Firstly, impedances $Z_{e,g,f}$ will be referred across the r_b: 1 transformer. This transformer will then be combined with the A'_{out}: 1 transformer, this then gives A_{out} (85) a similar definition to A_{in}. Additionally, Z_a and $Z_b$will be combined, as will Z_d and Z_e (after referring across r_b) impedances. The resulting circuit is shown in Fig. A.1.

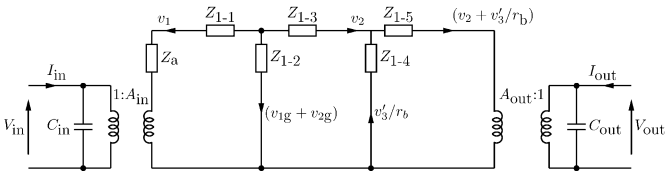

Fig. A.1. First stage of simplifications to the ring-dot equivalent circuit

The impedances $Z_{1\text{-}(1\text{-}5)}$ in Fig. A.1 are given by,

$$Z_{1\text{-}1} = Z_a + Z_b \tag{A.1}$$

$$Z_{1\text{-}2} = Z_c \tag{A.2}$$

$$Z_{1\text{-}3} = Z_d + Z_e r_b^2 \tag{A.3}$$

$$Z_{1\text{-}4} = Z_g r_b^2 \tag{A.4}$$

$$Z_{1\text{-}5} = Z_f r_b^2 \tag{A.5}$$

and A_{out} is now defined as,

$$A_{\text{out}} = A'_{\text{out}} r_b \tag{A.6}$$

The next stage of simplification requires transforming Z_{1-2}, $Z_{1\text{-}3}$ and $Z_{1\text{-}4}$ from a 'π' circuit to a 'tee' circuit. The resulting circuit is shown in Fig. A.2.

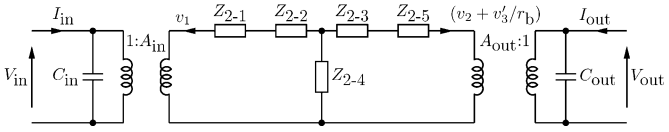

Fig. A.2. Second stage of simplifications to the ring-dot equivalent circuit

The impedances $Z_{2\text{-}(1\text{-}5)}$ in Fig. A.2 are given by,

$$Z_{2\text{-}1} = Z_{1\text{-}1} \tag{A.7}$$

$$Z_{2\text{-}2} = \frac{Z_{1\text{-}2} Z_{1\text{-}3}}{Z_{1\text{-}2} + Z_{1\text{-}3} + Z_{1\text{-}4}} \tag{A.8}$$

$$Z_{2\text{-}3} = \frac{Z_{1\text{-}2} Z_{1\text{-}4}}{Z_{1\text{-}2} + Z_{1\text{-}3} + Z_{1\text{-}4}} \tag{A.9}$$

$$Z_{2\text{-}4} = \frac{Z_{1\text{-}3} Z_{1\text{-}4}}{Z_{1\text{-}2} + Z_{1\text{-}3} + Z_{1\text{-}4}} \tag{A.10}$$

$$Z_{2\text{-}5} = Z_{1\text{-}5} \tag{A.11}$$

Then, combining impedances $Z_{2\text{-}1} + Z_{2\text{-}2}$ and $Z_{2\text{-}4} + Z_{2\text{-}5}$, leads to the equivalent circuit given in Fig. A.3.

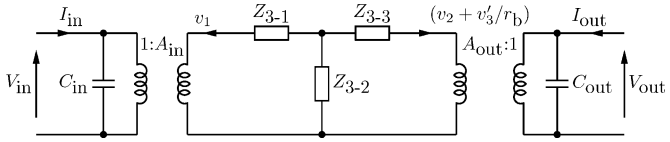

Fig. A.3. Third stage of simplification of the ring-dot equivalent circuit

The impedances $Z_{3\text{-}(1\text{-}3)}$ in Fig. A.3 are given by,

$$Z_{3\text{-}1} = Z_{2\text{-}1} + Z_{2\text{-}2} \tag{A.12}$$

$$Z_{3\text{-}2} = Z_{2\text{-}3} \tag{A.13}$$

$$Z_{3\text{-}3} = Z_{2\text{-}4} + Z_{2\text{-}5} \tag{A.14}$$

Again, a tee-to-π conversion will be performed on the three impedances $Z_{3\text{-}(1\text{-}3)}$ to give each impedance the same resonant frequency. This leads to the circuit shown in Fig. 11, with impedances $Z_{4\text{-}(1\text{-}3)}$ given by

$$Z_{4\text{-}1} = \frac{(Z_{3\text{-}1}Z_{3\text{-}2}) + (Z_{3\text{-}1}Z_{3\text{-}3}) + (Z_{3\text{-}2}Z_{3\text{-}3})}{Z_{3\text{-}3}} \tag{A.15}$$

$$Z_{4\text{-}2} = \frac{(Z_{3\text{-}1}Z_{3\text{-}2}) + (Z_{3\text{-}1}Z_{3\text{-}3}) + (Z_{3\text{-}2}Z_{3\text{-}3})}{Z_{3\text{-}2}} \tag{A.16}$$

$$Z_{4\text{-}3} = \frac{(Z_{3\text{-}1}Z_{3\text{-}2}) + (Z_{3\text{-}1}Z_{3\text{-}3}) + (Z_{3\text{-}2}Z_{3\text{-}3})}{Z_{3\text{-}1}} \tag{A.17}$$